A Numerical Study of The Quantum Backflow Effect

by

Samuel O'Mullane

Submitted to the Department of Theoretical Physics
in partial fulfillment of the requirements for the degree of

Master of Science in Quantum Fields and Fundamental Forces

at the

IMPERIAL COLLEGE LONDON

October 2013

Author .....
Department of Theoretical Physics
August 18, 2013

Certified by .....
Jonathan Halliwell
Professor
Thesis Supervisor

Accepted by .....

A Numerical Study of The Quantum Backflow Effect

by

Samuel O'Mullane

Submitted to the Department of Theoretical Physics
on August 18, 2013, in partial fulfillment of the
requirements for the degree of
Master of Science in Quantum Fields and Fundamental Forces

Abstract

In this thesis, I will describe the peculiar quantum backflow effect and go into detail regarding its numerical calculation. Backflow is described as a flow of negative probability and seems to be characterized by a new quantum number - the largest negative eigenvalue of the backflow operator. This effect is seen primarily in time of arrival calculations and though its description seems basic, it is of fundamental importance. Though experimental testing was not possible when backflow was first described in the 1960s, today there are groups working on confirming this phenomenon to high precision. I will begin with an overview of the backflow effect. Then, I will dive into the numerical detail and conclude with possible experimental realization.

Thesis Supervisor: Jonathan Halliwell
Title: Professor

Contents

List of Figures

Chapter 1

Introduction

1.1 The Origin of Backflow

Starting with Allcock's papers in 1969 [1, 2, 3] on issues relating to time of arrival in quantum mechanics, an interesting and controversial topic was first elucidated. In those papers, Allcock describes the phenomenon whereby, for simplicity, a one-dimensional wavefunction with purely positive momenta actually has decreasing probability of crossing the origin in some finite period of time. In classical mechanics, we are able to use the current as a distribution of when the particle will arrive at the origin (see fig.1-1a). The consequence of backflow is that this is not possible, because there is an area of negative probability (see fig.1-1b). Since my initial focus in this dissertation is numerical calculation of backflow itself, I will refrain from entering into the time of arrival controversy here - just know that the concept of backflow is crucial to understanding that sector of quantum theory.

1.2 A New Quantum Number

Following Allcock, there were no notable publications on backflow for many years. About 25 years later, Bracken and Melloy published their first and most important work on the subject. In that 1994 paper [4], backflow was clearly explained starting with where it came from, a few illustrative examples, scaling of the current and finally

Figure 1-1: Classical v. Quantum Probability

(a) Classical Probability

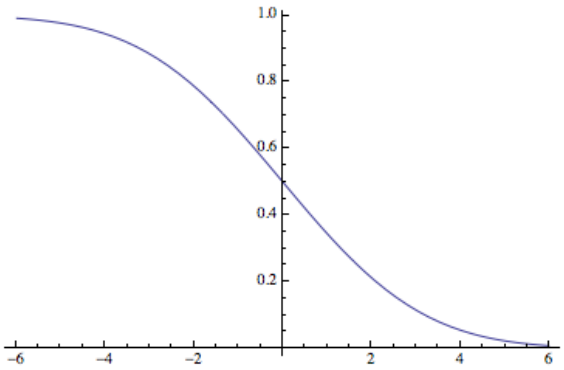

(b) Quantum Probability

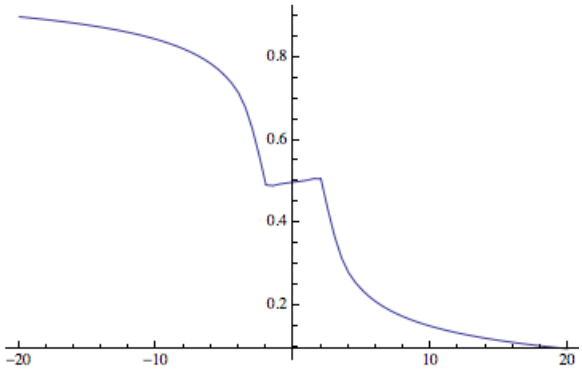

framing of the problem as an eigenvalue problem. Additionally, Bracken and Melloy introduced a new dimensionless quantum number that was the maximum negative probability flux a wavefunction could produce. What was remarkable was that this new quantum number did not depend on the mass, the time frame or even $\hbar$ and had no classical counterpart.

The next pivotal paper on backflow was produced by Penz et. al. in 2006. In this paper [7], many important properties of backflow are derived. By formulating the problem in terms of operators, it is shown that the backflow operator must be linear bounded, self-adjoint and non-compact. Additionally, an algorithm is described that is useful to speed up all necessary calculations of the ideal backflow system. The numerical results produced for the paper to this day serve as the standard for backflow calculation and visual comparison. By reproducing these results, we can be sure that our calculations on trial wavefunctions will be accurate.

Again since my primary focus in this thesis is the numerical work, I will leave the literature review until later. In the next chapter we will jump back through some of the papers and rederive what has been stated in this introduction as given.

Chapter 2

Numerical Beginnings

As there is no known analytic solution to the backflow problem, numerical calculations are essential for understanding and progressing the phenomenon. We will begin our discussion from the first principles of the backflow problem and then work through the various computational methods used to solve it. Note that much of the following has been rederived from Bracken Melloy [4] and Penz [7].

2.1 Formulation of the Backflow Problem

As detailed by most authors who cover this problem, the problem we are attempting to solve is this:

When a free particle with a normalized wavefunction Ψ(x,t) is moving on the x-axis with strictly positive momenta, its current j(x,t) may be negative over some finite time.

Note that the current is defined as

$$j(x,t) = -i\frac{\hbar}{2m}[\Psi^*(x,t)\frac{\partial\Psi(x,t)}{\partial x} - \frac{\partial\Psi^*(x,t)}{\partial x}\Psi(x,t)] \tag{2.1}$$

while the probability density is given by

$$\rho(x,t) = \Psi^*(x,t)\Psi(x,t) \tag{2.2}$$

such that the conservation equation

$$\frac{\partial \rho(x,t)}{\partial t} + \frac{\partial j(x,t)}{\partial x} = 0$$

holds as required by the Schrodinger equation for a free particle.

Also, note that the probability that the particle has not crossed the origin (is in $x < 0$) is related to the quantum mechanical current by the equation

$$\frac{dP(t)}{dt} = -j(0,t).$$

Moving to momentum space with the assumption that all momenta are positive via the transformation

$$\Psi(x,t) = \frac{1}{\sqrt{2\pi\hbar}} \int_0^\infty e^{\frac{ixp}{\hbar}} e^{\frac{-ip^2 t}{2m\hbar}} \phi(p)\, dp \tag{2.3}$$

we see that backflow occurs for any free particle with normalized ϕ(p) which vanishes for $p < 0$ and has negative current j(0,0). The reason only j(0,0) need be negative is that continuity requires that j(0,t) is also negative over some finite time interval [0,T).

2.2 Eigenvalue Framework

When the general form for $\Psi(x,t)$ given by equation 2.3 is used to calculate the current, we find

$$j(0,t) = \frac{1}{4\pi m\hbar} \int_0^\infty \int_0^\infty (p+q) e^{i(p^2-q^2)t} 2m\hbar \phi^*(p)\phi(q)\, dp\, dq \tag{2.4}$$

Integrating this to find the flux, in this case the amount of backflow, we have

$$\Delta_p = P(T) - P(0) = -\int_0^T j(0,t)\, dt$$

which after integrating over t, gives us

$$\Delta_p = \int_0^\infty \int_0^\infty \phi^*(p) K(p,q) \phi(p)\, dp\, dq \tag{2.5}$$

where the kernel K is defined as

$$K(p,q) = \frac{i}{2\pi}\left[\frac{e^{\frac{i(p^2-q^2)T}{2m\hbar}} - 1}{p-q}\right]$$

Now since we are looking to maximize the amount of backflow, we must consider the maximum of the functional

$$I(\phi) = \int_0^\infty \int_0^\infty \phi^*(p) K(p,q) \phi(p)\, dp\, dq - \lambda \int_0^\infty \phi^*(p)\phi(p)\, dp$$

where we have introduced the Lagrange multiplier λ.

With all of this framework and the Euler-Lagrange equation given by

$$\int_0^\infty K(p,q)\phi(q)\, dq = \lambda\phi(p)$$

we see immediately that the multiplier and the backflow flux are related by

$$\lambda = \Delta_p$$

thus our original problem of maximizing backflow is now entirely an eigenvalue problem. After a suitable change of variables, we can write this explicitly as

$$\frac{1}{2\pi}\int_0^\infty \frac{sin(u^2 - v^2)}{u - v}\phi(v)\, dv = -\lambda\phi(u) \tag{2.6}$$

2.3 Discrete Summations and Matrix Computations

As detailed in [17], integral eigenvalue equations of this kind are known as Fredholm equations of the second kind. Though perhaps not analytically soluble, they can always be calculated using discrete summation methods. In a general sense, these methods all involve breaking up the integral into manageable pieces and then extrapolating out to the final answer. In our case, the eigenvalue is the main concern and thus we encode the integral information into an appropriately sized matrix and then use a subroutine that finds the eigenvalue. The numerical details can be tedious and information on the algorithms used to solve these equations is left in [17].

2.3.1 Matrix Eigenvalue Calculation

Since the amount of backflow is the most important aspect of our calculations, we will begin with that calculation. Because analytical integration is not possible here, we must resort to numerical methods specifically discretizing the integral. Using the algorithm described in Bracken and Melloy [4], below is an appropriate implementation that is quite accurate.

```
h = 2;
q0 = 10;
n0 = 500;
q = q0*h^.5;
n = n0*h;

v[x_] := q (x - 1.)/n;

k = Table[
   If[i == j, 2 v[i]/Pi, 1/Pi Sin[v[i]^2 - v[j]^2]/(v[i] - v[j])], {i,
     n}, {j, n}];
```

```
If[n0 - 8.*q0^2/Pi > 0,
 1 - Max[Eigenvalues[IdentityMatrix[n] - k*q/n]], "error"]
```

Basically this program takes the desired integration but instead of integrating from zero to infinity, only sums to the value of q with finite step size q/n where n is the number of points sampled. The result is an n by n matrix, in this case 1000 by 1000, which although slow to compute, is fairly accurate. The output for the above code is -0.0369736 which is within 4% of the actual answer.

Though somewhat accurate, the way Bracken and Melloy found out the maximum backflow flux was by computing these matrices for various values of h and then fitting a curve to find the true value for the integration. Their findings were not completely correct because they used an improper fit, but later Penz [7] fit the correct curve by plotting λ versus $\frac{1}{\sqrt{h}}$ and fitting a third order polynomial to the line. Penz's final answer, though computed with a different method, was -0.0384517.

When I reproduced Bracken and Melloy's method and applied Penz's line of best fit, the result is -0.03845, which is rather accurate. The plot I used is pictured below.

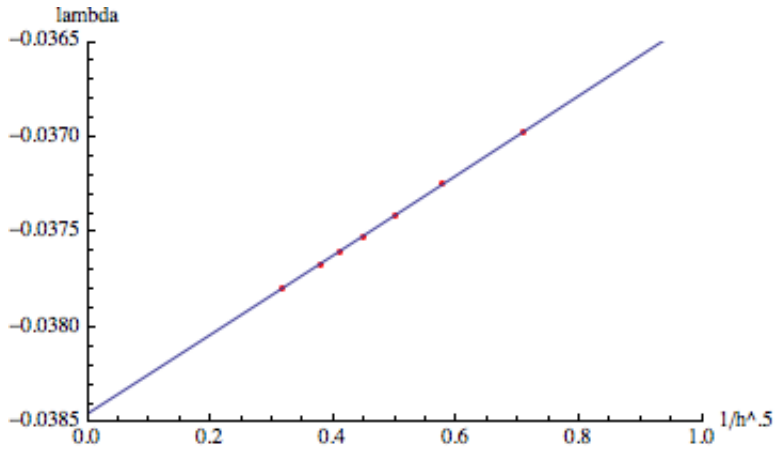

Figure 2-1: $h^{-.5}$ plotted against λ

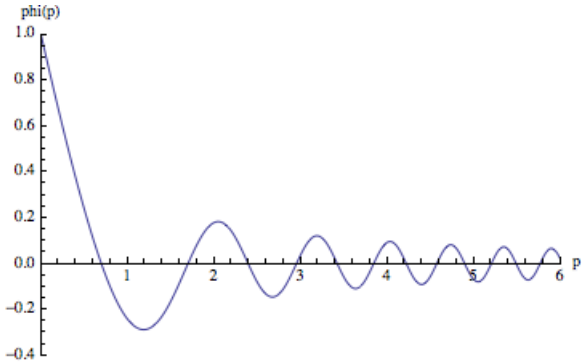

Figure 2-2: The h=1 eigenvector in momentum space

2.3.2 Matrix Eigenvector Calculation

As the introduction states, the focus today is not on improving the accuracy of our backflow eigenvalue calculation, rather searching for the analytical eigenvector or solutions that are very near it. With the aid of Mathematica's built in subroutines, we can take the program from the last section, change "eigenvalues" to "eigenvalues" and find the exact numerical solution. From this, we may compare our various guesses and additionally compute other required and interesting quantities such as the current and the probability.

```
eigvec = If[n0 - 8.*q0^2/Pi > 0,
   Eigenvectors[IdentityMatrix[n] - k*q/n, 1], "error"];
```

While it may seem as if changing the value of h may give vastly different eigenvectors, the surprising quality of the backflow maximizing vector is that it is almost entirely unchanged by such a shift. Below is a comparison between h=1 and h=4.

Looking at the above momentum space eigenvector, we see clearly that the wavefunction fulfills our previous condition of vanishing for $p < 0$. The other noticeable feature is its highly oscillatory nature, which makes numerical integrations difficult - something that will be discussed later on. With these preliminary results, it would be nice to improve the accuracy of our calculation so that we can be sure our comparisons with possible analytic solutions are accurate as well. Here we turn to Penz's improved algorithm from 2006 and the operator form used.

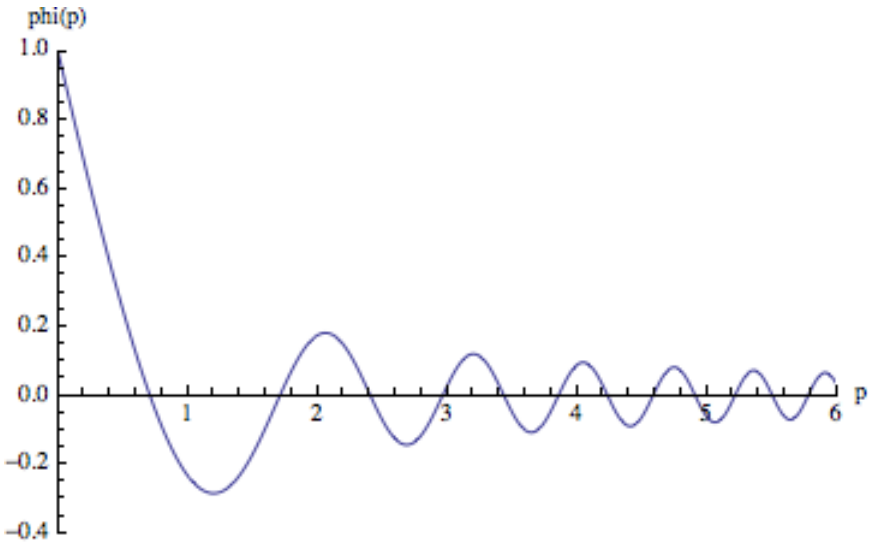

Figure 2-3: The h=4 eigenvector in momentum space

Chapter 3

The Backflow Operator

In the previous chapter, we saw how Bracken and Melloy, and later Eveson et. al. [6] used the integral operator K to calculate the maximal backflow state. In 2006, Penz et. al. [7] described a method that independently confirmed these results via an operator formulation and the power method for numerical efficiency. In addition to reproducing these results, we will look at the conditions and stipulations on the backflow operator that were detailed in that paper.

3.1 Definitions and Propositions

In order to appropriately cover this subject, many definitions will be needed. Our space will be $L^2(R)$ which is the space of square integrable functions. Rescale the time as

$$t = \hbar t_{phys}/(2m)$$

where t is real. We term the free Schrodinger evolution $U_t : L^2(R) \to L^2(R)$ from time 0 to t as:

$$(U_t\phi)(k) = \phi_t(k) := exp(-ik^2t)phi(k)$$

Denote the inverse L^2-Fourier transform of ϕ_t as

$$\psi_t(x) := (F^*\phi_t)(x) = \frac{1}{2\pi}\int_{-\infty}^{\infty} exp(ikx)\phi_t(k)\,dk$$

Since we will need an analogue of the Heaviside Theta function, define $\Pi : L^2(R) \to L^2(R)$ with

$$(\Pi f)(x) = \begin{cases} f(x) & : x > 0 \\ 0 & : x < 0 \end{cases}$$

Then if the momentum space wavefunction is normalized as usually expected, we can write the probability that a measurement at time t reads a position $x > 0$ as

$$P(\phi_t) := \int_0^\infty |\psi_t(x)|^2 \, dx = \langle \phi_t, F\Pi F^* \phi_t \rangle$$

The probabilities for spaces and functions such as these given obey $P(\phi_t) \to 0$ for $t \to -\infty$ and $P(\phi_t) \to 1$ for $t \to \infty$ according to Dollard's lemma [8]. However, it is possible that the probability does not increase monotonically from 0 to 1 and can in fact decrease over any number of separate time intervals. During these intervals, given $s < t$ we can write

$$\lambda(\phi) := sup\{P(\phi_s) - P(\phi_t)\} > 0$$

where *sup* designates the supremum of the set. Likewise, we can define the "backflow constant" i.e. the maximal backflow allowed as

$$\lambda := sup\{\lambda(\phi)\}$$

.

Next define the transformed projection operator $\tilde{\Pi}_t := U_t^* F \Pi F^* U_t$ which allows us to write

$$P(\phi_s) - P(\phi_t) = \langle \phi, (\tilde{\Pi}_s - \tilde{\Pi}_t)\phi \rangle$$

then we can infer that

$$\lambda = sup\{\langle \phi, U_\tau^* (\tilde{\Pi_{-T}} - \tilde{\Pi_T}) U_\tau \phi \rangle\}$$

and with the definition of the backflow operator $B_T := \tilde{\Pi_{-T}} - \tilde{\Pi_T}$, we find that

$$\lambda = sup\{\sigma(\Pi B_T \Pi)\} \tag{3.1}$$

for all $T > 0$. Since this result can easily be shown to be independent of scaling, we have shown that this equation holds for any T and we will thus choose $T = 1$ out of convenience.

3.2 Equivalence of Methods

Though I will not dive into the details of the equivalence between this treatment and the treatment in Bracken and Melloy, I will briefly summarize it. First define the square integrable Hilbert transformation as

$$(Hf)(k) = \frac{1}{\pi} P \int_{-\infty}^{\infty} \frac{f(q)}{k-q}\, dq$$

Then it can be derived that $F\Pi F^* = 1/2(-iH + id)$ where id is the identity operator. It follows that $B = -i/2(UHU^* - U^*HU)$ and consequently our main result:

$$(\Pi B \Pi \phi)(k) = -1/\pi \int_0^{\infty} \frac{sin(k^2 - q^2)}{k-q} \phi(q)\, dq = (K\phi)(k) \tag{3.2}$$

. This confirms that the two treatments are in fact the same and that our calculations will hold if we use this formalism. By using this technique, Penz et. al. additionally found that the backflow operator is required to be non-compact.

3.3 The Power Method

As previously stated, the results produced by Penz were superior not only because of the improved accuracy but also the efficiency of the calculations. These improvements were achieved through use of the power method. From [12], we see that this method is computationally much simpler while producing more accurate results.

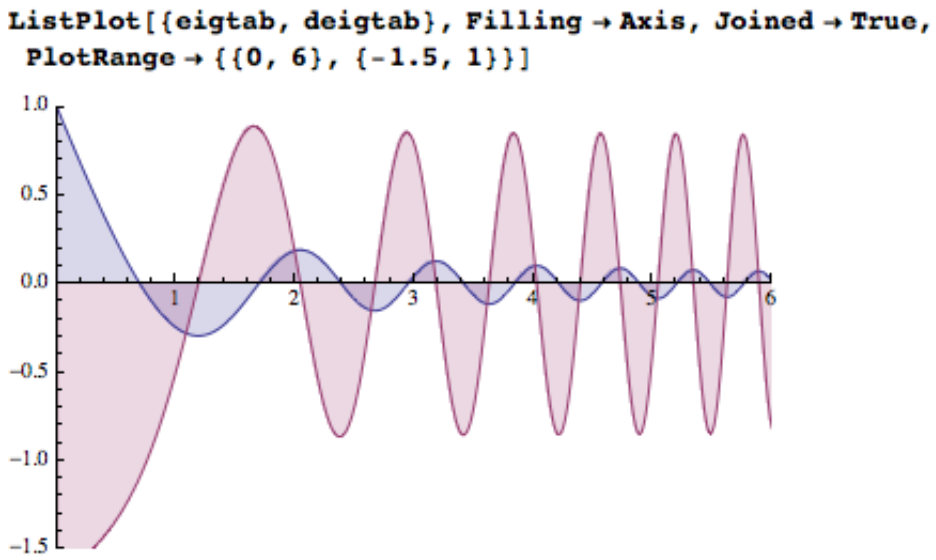

Figure 3-1: Backflow Maximizing Eigenvector in Momentum Space with Derivative

The basic idea (rederived from [10, 11]) is to take an initial vector and then apply the recursive relation $v_{n+1} = \frac{1}{||v_n||} A v_n$ through a loop and then find the eigenvalue

$$a = \lim_{n \to \infty} v_{n+1}^{\dagger} \frac{v_n}{||v_n||}.$$

Note that this program was tested for various different starting vectors and the results were exactly the same, so the initial vector is not important within reason.

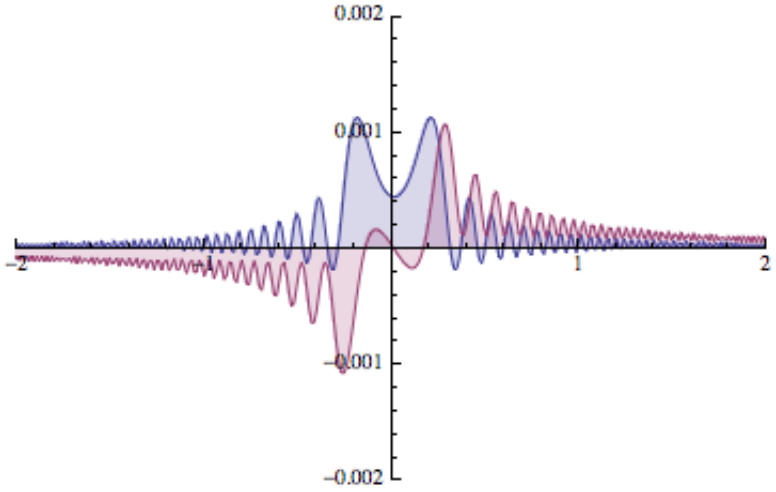

Figure 3-2: Backflow Maximizing Eigenvector in Coordinate Space, Real and Imaginary Parts, t = 0

Since this is applied to the operator $\Pi B \Pi + id$, the largest eigenvalue approximates $\lambda + 1$ while the eigenvector output is the correct backflow maximizing state in momentum space. The code for the implementation of this method can be found in appendix A. The other important result from Penz's paper was that the backflow maximizing state decays faster than $sin(k^2)/k$, showing that it is indeed square integrable.

```
ListPlot[currtab, DataRange → {-5, 5}, Joined → True,
 PlotRange → {{-3, 3}, {-.05, .08}}]
```

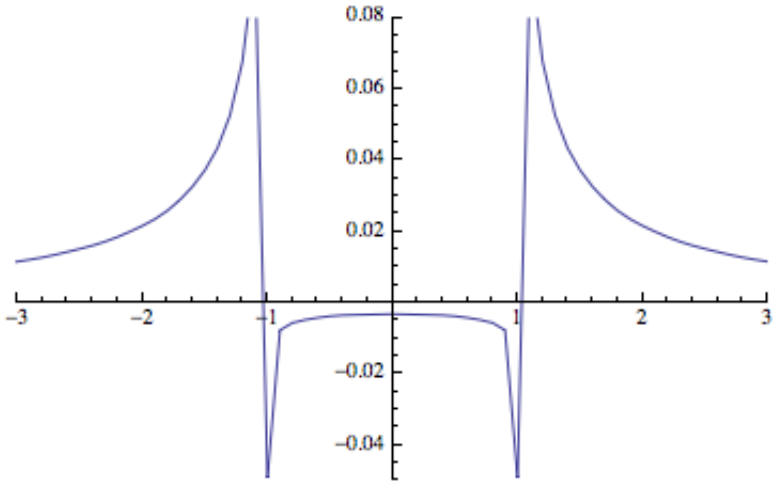

Figure 3-3: Ideal Current for Backflow Eigenvector

The figures in this chapter were produced through this program and show important features of the backflow maximizing states. For the coordinate space wavefunction, we see that the real part is symmetric about the y-axis whereas the imaginary part is antisymmetric. Additionally, we see that there is an actual discontinuity in the current at $t = \pm 1$ and that in that area around the origin, the current is negative. When this is integrated over, it provides the required ideal backflow maximizing flux. Note that the pictured current doesn't show a sharp discontinuity due to the reduced step size used to produce that plot.

Chapter 4

The Search for an Analytic Solution

As our primary goal with this thesis is to try and find the analytical solution to the backflow maximizing problem, it is best if we now look at guesses that have been attempted recently, including work produced exclusively for this thesis.

4.1 Required Properties for Approximate Solutions

Looking through the detailed work of Penz et. al. in conjunction with Bracken and Melloy's treatment allows us to formulate a list of required properties for our ideal solution.

1. Momentum space wavefunction is zero for $p < 0$ and decays in amplitude for $p > 0$

2. Coordinate space wavefunction has an even real part and an odd imaginary part This is derived from analyzing Bracken and Melloy's integral kernal; since it is real, the above must hold.

3. Current has an area of strictly negative flux between $t = \pm 1$

4. Current is singular in nature at the boundaries $t = \pm 1$

Figure 4-1: Guess 1 in momentum space (blue) plotted with the eigenvector (red)

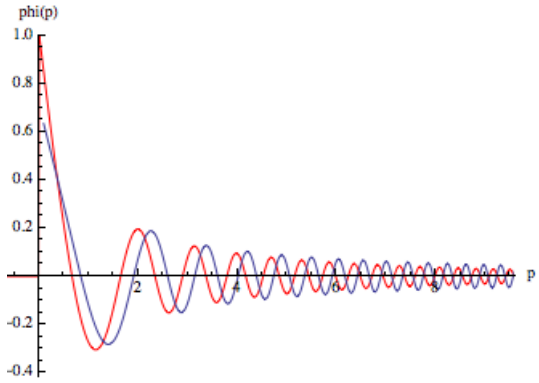

5. Invariance under the combined parity and time reversal operation

4.2 Yearsley's Two Guesses

In 2012, a paper was published by Yearsley et. al. [9] detailing the backflow problem and specifically several attempts at an analytic solution. The two numbered guesses will be discussed here for proof of concept but not detailed in calculation.

First, the following wavefunction was proposed:

$$\phi_1(u) = N\sqrt{\frac{2}{\pi}}\int_1^\infty u(\cos(z^2u^2) + a\sin(z^2u^2))\,dz. \tag{4.1}$$

The function is easily normalized and for the choice of $a = 0.4$, we have an approximate backflow maximizing state. Using suitable change of variables, the authors rewrote the current from

$$J(t) = Re(1/\pi\int_0^\infty \exp(itu^2)\phi(u)\,du\int_0^\infty v\exp(-itv^2)\phi(v)\,dv)$$

to $J(t)1/\pi Re(U(t)V(t))$ which allows for easy current calculation analytically. Looking at the above wavefunction, one would think that this guess is not terribly accurate but the flux calculations show that this state exhibits 55% maximal backflow at $F = -0.02095$. Additionally, the current is actually remarkably visibly similar, showing that the momentum space wavefunction can be deceiving when trying to

come up with close analytical guesses.

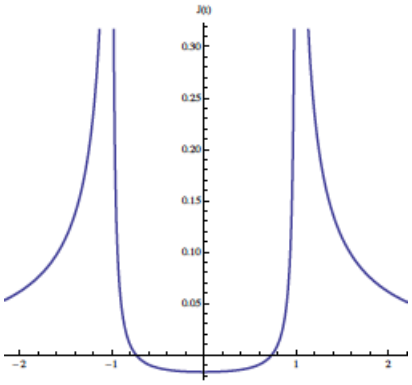

Figure 4-2: Current for Guess 1 with a = .4, $\epsilon = 10^{-7}$ from REF=yearsley

Note that the epsilon listed for the current was used in analytical integration to make the integral converge. Another important part of this guess was the asymptotic form, which for large u is

$$\phi_1(u)\ N\left(-sin(u^2)/u + a\,cos(u^2)/u\right)$$

. This is important because of the previous analysis from Penz showing that the wavefunction should decay faster that $sin(u^2)/u$, so using something with that approximate form is a good choice.

The second guess proposed in the paper was much closer visually to the backflow maximizing eigenvector. The wavefunction for this guess is:

$$\phi_2(u) = N\left(aexp(-bu) + (1/2 - C(u))\right) \tag{4.2}$$

where a and b are real and the function C is the Fresnel integral function defined by

$$C(u) = \sqrt{2/\pi}\int_0^u cos(x^2)\,dx.$$

After normalization and optimization, it is found that $a = 0.6, b = 2.8$ and $\epsilon = 10^{-7}$ are the backflow maximizing constants here. Much like the eigencurrent, the current produced for this guess has a pronounced curve in the negative flux area,

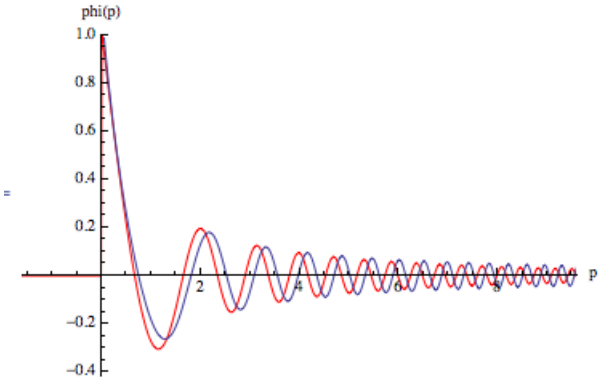

Figure 4-3: Guess 2 in momentum space (blue) plotted with the eigenvector (red)

Figure 4-4: Current for Guess 2 with a = 0.6, b = 2.8, $\epsilon = 10^{-7}$ from REF=yearsley

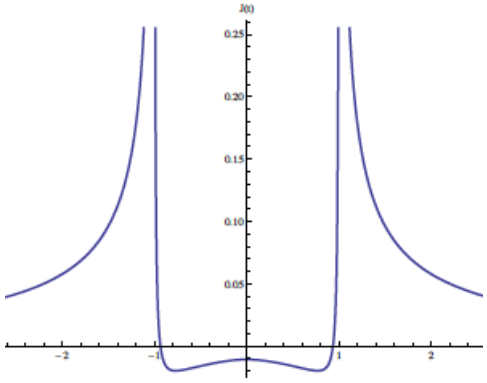

showing improved agreement over the last guess.

The flux calculated for this state was $F = -0.02757$ which is about 70% of the maximum. It appears that these guesses may be along the correct path towards a final analytic solution. Using some of the methods developed through their work, we will now go on to discuss our own work and possible solutions.

4.3 Decaying Exponential

As suggested by Prof. Halliwell, this guess is an attempt to find a simple wavefunction that is easily integrable and analyzable. In momentum space, this function is:

$$\phi(p) = N\,(a - p)e^{-bp^2}\Theta(p) \tag{4.3}$$

Note that the $\Theta(p)$ denotes the Heaviside step function as usual. After straightforward integration, we find that the normalization is given as a function of a and b as:

$$N = \frac{4}{\sqrt{-8ab^{-1} + b^{-3/2}(2\pi)^{1/2} + 4a^2b^{-1/2}(2\pi)^{1/2}}}$$

After finding the combination of $a = 2.2$ and $b = 0.1$ that maximize backflow, we find that $N_{max} = 0.5311$. Using equation (2.3), we find the Fourier transform in dimensionless units to be:

$$\psi(x,t) = \frac{N}{\sqrt{4\pi}} \frac{\exp(-\frac{x^2}{4b+2it}) \left(\sqrt{\pi}(2iab - at + x)(\text{ Erfi}\left[\frac{x}{\sqrt{4b+2it}}\right] - i) - \exp(\frac{x^2}{4b+2it})\sqrt{4b+2it}\right)}{(2b+it)^{3/2}} \tag{4.4}$$

In this Fourier transform we have used the imaginary error function denoted Erfi which is defined as Erfi[x] = Erf[i x]/x. For those unfamiliar, the error function is defined as the integral of the Gaussian distribution, meaning

$$\text{Erf[x]} = \frac{2}{\sqrt{\pi}} \int_0^x exp(-t^2)\, dt$$

As we see in the time evolution plots of $\psi(x,t)$ above, the wavefunction has the required form for coordinate space, i.e. the real part is symmetric and the imaginary part is antisymmetric about the y-axis.

If we compare these wavefunctions with the ideal ones, we see that there lack

Figure 4-5: Decaying Exponential $\phi(p)$ (blue)

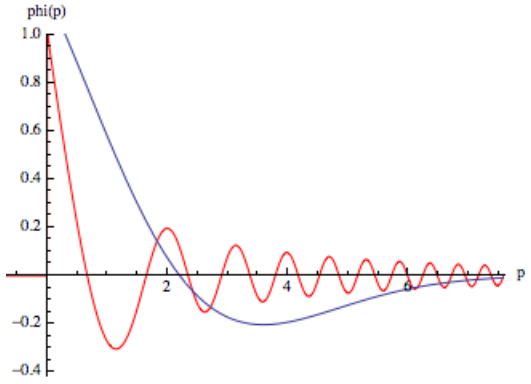

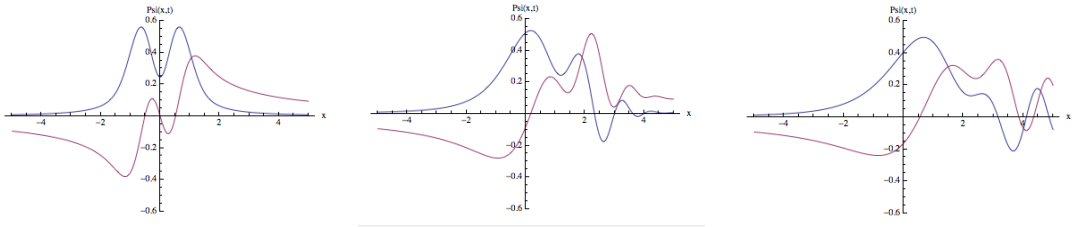

(a) $\psi(x, 0)$ (b) $\psi(x, 0.5)$ (c) $\psi(x, 1)$

Figure 4-6: Time Evolution of $\psi(x, t)$ (real part = blue, imaginary = red)

the characteristic oscillations that make up the backflow maximizing state. This was expected because our trial function is simply a decaying exponential and it is remarkable that such a simple state can still exhibit so much backflow. Additionally, figure 4-7 is a three-dimensional plot showing the general behavior near the origin in both space and time directions.

It is also informative to consider the probability density of this wavefunction. As is standard in quantum mechanics calculations, we will use equation (2.2) to produce the plots seen in figure 4-8.

The plots of the probability density and real part of the coordinate space wavefunction are nearly Gaussian with a divot around the origin. The fact that these simple, experimentally realizable functions mean that future experiments to demonstrate the reality of the backflow effect can be rather simple. As seen in the literature, the superposition of 2 or more Gaussian shapes easily produces the backflow effect, albeit with noticeably submaximal negative probability flux.

As with all backflow calculations, the most important result is the current. In the other plots we have seen so far, the current has a Gaussian shape except for

Figure 4-7: Plot of $\psi(x, t)$ in 3D

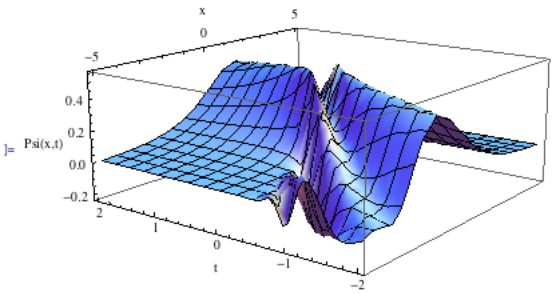

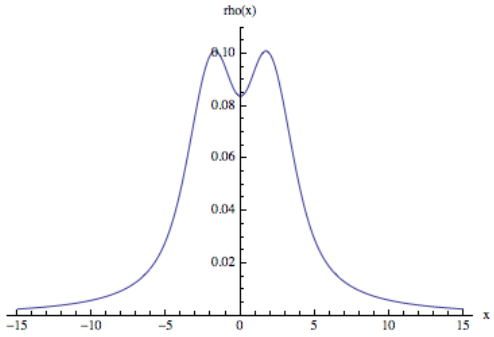

(a) $\rho(x, 0)$

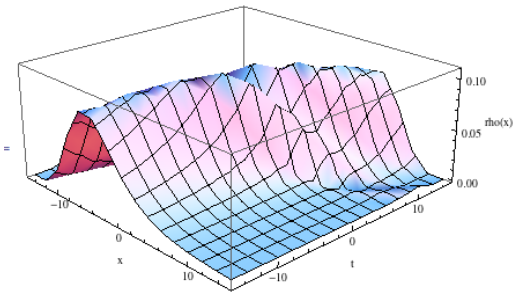

(b) $\rho(x, t)$

Figure 4-8: Plots of $\rho(x, t)$

Figure 4-9: J(t) v. t for the decaying exponential

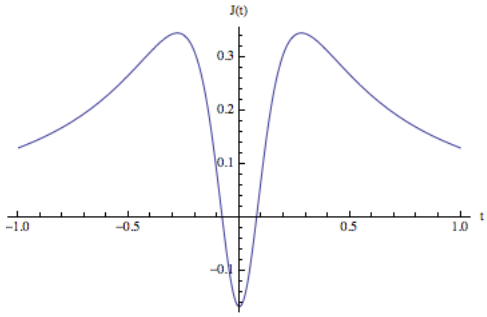

between $t = \pm 1$ where there is some bizarre behavior including two discontinuities and a mostly flat, slightly curved surface. With this trial function, we see no flat surface but rather a curve that resembles a Gaussian with its middle pushed down below the x-axis. When tuning the parameters a and b, this was most evident. For $0 < a < 1$ and $a > 6$, the current is reminiscent of a Cauchy distribution, i.e. there is no irregularity at the origin. As a is tuned closer to its "correct" value of 2.2, the curve around the origin deforms lower, passing the y-axis and reaching what is pictured in the provided plot. While there may be further numerical analysis of this function from applied mathematics or statistics, currently we do not have much information on why this occurs.

Looking at the plots of the probability, it appears that there is only a tiny amount of backflow. Quite surprisingly, our calculations show a negative probability flux of $F = -0.01657$ which is about 43% of the maximum, only 10-15% off of the first guess of Yearsley. With this remarkable result, we know that even simple looking

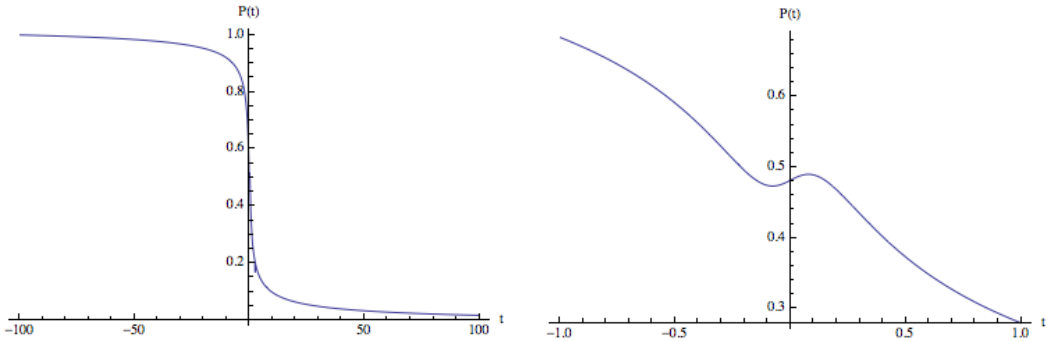

(a) P(t) over [-100,100] (b) P(t) over [-1,1]

Figure 4-10: Plots of P(t)

states that appear to have minimal backflow may in fact have a large percentage of maximum backflow - good news for the experimentalists who wish to measure this quantity. Note that in the above calculations the probability shown is the probability that a measurement shows $x < 0$ which is opposite of the convention used by some other authors.

Chapter 5

The Airy Trials

On my own hunch, I have decided to investigate a function that may lead us closer to the analytical solution for the backflow problem. The wavefunctions I will discuss in this chapter will be based on the Airy functions seen in optics and semi-classical mechanics. It is due to their highly oscillatory behavior and suitable asymptotic behavior that I chose them - simply speaking, they are visually very similar in momentum space to the backflow maximizing eigenvector.

But many functions can be tuned to look like the backflow maximizing states, why should we look at Airy functions? Because the Airy trial-wavefunctions satisfy nearly all of the points in the list for ideal backflow maximizing states detailed in chapter 4. As I will detail throughout this chapter, these functions have appropriate oscillating coordinate space wavefunctions (with the correct symmetry) as well as very interesting current behavior. Hopefully these results will lead to a greater understanding of the quantum backflow effect and shed some light on where these functions may originate from.

5.1 Momentum Space

The Airy functions are well known in physics, particularly in optics, electromagnetics and specifically radiative transfer due to their differential equation definition [22].

The functions $Ai(x)$ and $Bi(x)$ are the two linearly independent solutions to

$$\frac{d^2y}{dx^2} - xy = 0. \tag{5.1}$$

The formal notation for these solutions involves hypergeometric functions, but for our use, the integral form is more informative [22]:

$$Ai(x) = \frac{1}{\pi}\int_0^\infty \cos(\frac{t^3}{3} + xt)\, dt$$

$$Bi(x) = \frac{1}{\pi}\int_0^\infty [exp(-\frac{t^3}{3} + xt) + \sin(\frac{t^3}{3} + xt)]\, dt$$

Taking a look at the plots of these functions, we see that our trial should focus on the region $x < 0$.

Figure 5-1: Airy Ai and Bi Functions

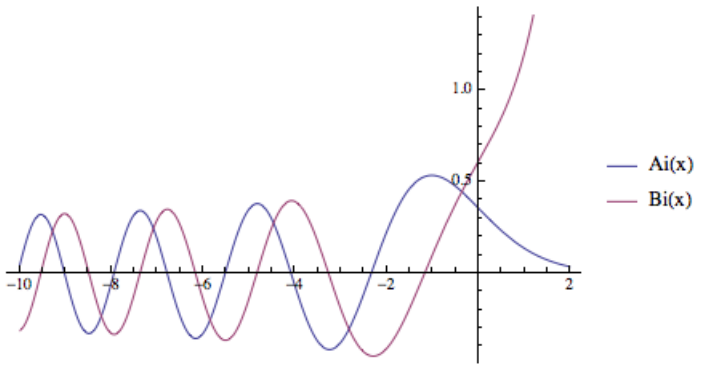

Another reason why Airy functions are a good choice for our trial wavefunction is their asymptotic behavior. For large negative values of z along the real axis, we have: [21]

$$\begin{aligned} Ai(-x) &\to \frac{\sin(2/3\, x^{3/2} + \pi/4)}{\sqrt{\pi}x^{1/4}} \\ Bi(-x) &\to \frac{\cos(2/3\, x^{3/2} + \pi/4)}{\sqrt{\pi}x^{1/4}} \end{aligned} \tag{5.2}$$

Since Penz et. al. showed that the backflow maximizing eigenvector is approximately asymptotic to $\sin(x^2)/x$, we will tailor our guess appropriately. Note that

these functions are equivalently useable for our purposes.

Because of its behavior near the origin, we choose now to look at the $Ai(-x)$ function alone. After adjusting several variables for optimal momentum space matching, we find that the function

$$\phi(p) = N \frac{Ai(-a\,(p+b)^{\frac{4}{3}})}{(p+b)^{\frac{2}{3}}} \tag{5.3}$$

works best with $a = 1.178$ and $b = 0.82$, leading to a normalization factor of $N = 2.14$.

Figure 5-2: Trial Function in Momentum Space

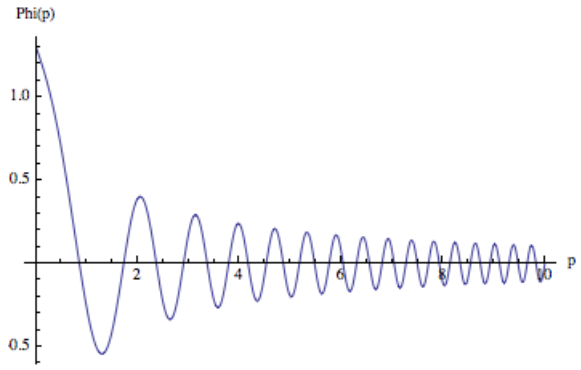

From the above asymptotic solution for the Airy Ai(-x) function, as p becomes large, we find that our trial wavefunction goes as:

$$\phi(p) \rightarrow \frac{\sin[2/3\,a^{\frac{3}{2}}\,(p+b)^2 + \pi/4]}{\sqrt{\pi}\,a^{\frac{1}{4}}\,(p+b)}$$

which is acceptable asymptotic behavior as required by Penz et. al. While this is obviously a good approximation in momentum space, the success or failure of this trial will be determined by the coordinate space results that follow.

5.2 Coordinate Space

We begin with the familiar Fourier transform equation from momentum to coordinate space:

$$\Psi(x,t) = \frac{1}{\sqrt{2\pi}} \int_0^\infty exp(ixp/\hbar) exp(-ip^2 t/2) \phi(p)\, dp$$

Figure 5-3: Trial Function in Coordinate Space - x-dependence

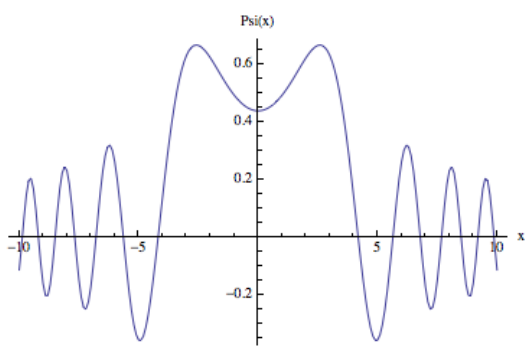

(a) The Real Part of $\Psi(x,0)$

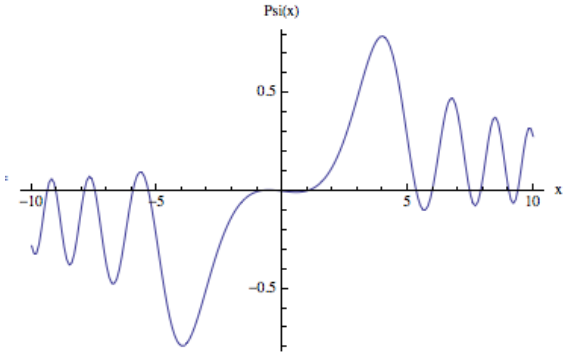

(b) The Imaginary Part of $\Psi(x,0)$

Figure 5-4: Trial Function in Coordinate Space - t-dependence

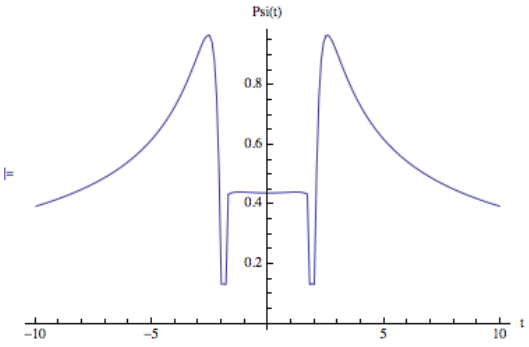

(a) The Real Part of $\Psi(0,t)$

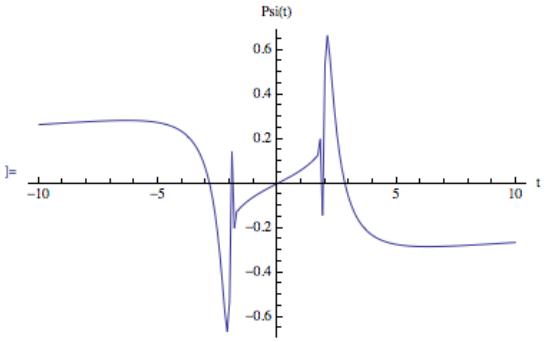

(b) The Imaginary Part of $\Psi(0,t)$

Note that from this point on, all work is numerical as the analytical calculations become quite difficult quickly. As seen in the given coordinate space graphs, the real part of the trial wavefunction is symmetric while the imaginary part is antisymmetic. This matches the behavior of the ideal case as seen in figure 3-2 (p.22). Additionally, the oscillatory nature in coordinate space is preserved and even the zeros appear to be consistent with the ideal case after appropriate scaling.

In addition to the x-space Fourier transform, we have additionally the t-space transform. While rarely mentioned or graphed in the literature, these two functions are crucial to calculating such quantities as the current or the probability density. From both of these graphs we see odd behavior about the origin. It appears that some discontinuity is occurring and the numerics are approximating it with very fast

oscillations. Though not thoroughly investigated, it is possible that these peculiarities are related to the Gibbs phenomenon - those strange oscillations and overshoots that accompany Fourier transforms of functions near discontinuities.

With the coordinate space wavefunction in hand, we can immediately find the current via $J(x,t) = \Im[\Psi^*(x,t)\nabla\Psi(x,t)]$ though understanding our results will require much effort.

5.3 Current Basics

Now looking at our plots of Ψ(x,t), we can see that our calculations are going to be rather messy around $t = \pm 2$. We will naively calculate the current anyway to see what happens.

Figure 5-5: Broad View of the Current

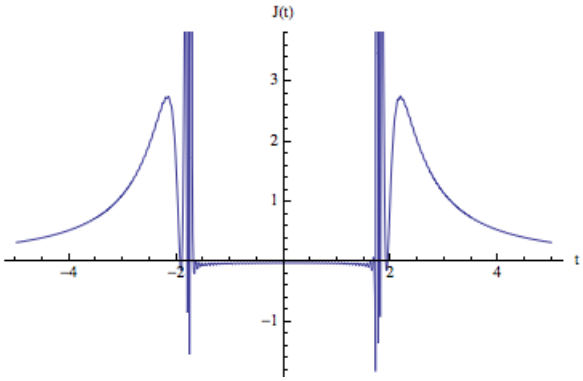

At this point it is instructive to note the good points of our results. First, we see that the tail behavior is appropriate with Gaussian-like fall off that decays rapidly. Second, some divergent behavior appears to be popping up near $t = \pm 2$ which is certainly a result of the applied gradient to the near discontinuous wavefunction near those points. This is encouraged due to the asymptotic behavior of the ideal current near $t = \pm 1$ though it make calculations tricky. Third, the behavior in between $t = \pm 2$ possibly has the shape we desire, though a closer look is necessary to confirm.

The main problem that we will have to address when calculating the maximum negative flux for this system is the appearance of large spikes both in the negative and

Figure 5-6: Problem with the Trial Current

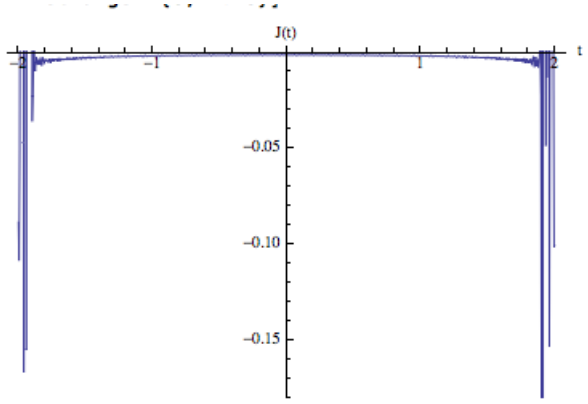

positive current sectors. If we simply ignore these spikes, our results are nonsensical and unphysical, showing either tiny or supermaximal amounts of backflow. Through the development of two purely original algorithms, I will first filter out some "noise" seen between $t = \pm 2$ and then smooth out the entirety of the current curve so that our calculations maintain the integrity of the full current calculations.

5.4 Current Approximations

5.4.1 Introduction

When we perform the above current calculations, the current is derived directly from the momentum-space wavefunction. As a result, the coordinate-space wavefunction is bypassed and the only curve that needs to be smoothed is the current. Since the integration is numerical and computationally extremely expensive, it is necessary to discretize. The results are pictured in the associated figures. It is interesting to note the appearance of three candidate curves for approximation in addition to the unadulterated curve: the minimal, the maximal and the mean curves. Note that the minimal curve appears to produce the most backflow and even resembles the ideal curve in shape.

We can immediately discard the idea of using the full curve because the numerical programs used to calculate the integrals of the current can not handle such wildly

Figure 5-7: Zoom of Current Between $t = \pm 2$

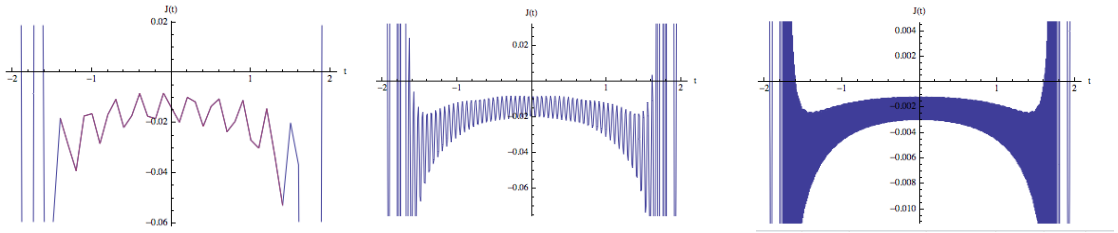

(a) Step Size of 0.1 (b) Step Size of 0.01 (c) Step Size of 0.001

oscillating functions. Thus begin our trials for noise filtration.

In order to guarantee that our results are not dependent on our smoothing function, we will perform calculations based on all three of the given curves and introduce one more possible curve that is close to the mean curve. Since the three plotted curves can easily be derived from their names, we will focus on this final unpictured curve. Because our whole procedure is based upon taking reasonable estimates of very unpredictable data, this final curve compromises by comparing the maximal and minimal curve and producing a reasonable estimate that is neither the mean nor a choice of either of the input curves. The exact details of this algorithm I developed are omitted to conserve space since the results will be in good agreement with other more readily confirmable calculations.

Analyzing the given maximal and minimal curves, we see that the middle noise has been heavily reduced to thin, accurate curves while the areas between $1.9 < |t| < 2$ are still problematic. So while one problem is essentially solved, the original large spikes remain. For the three plotted curves, we must then arbitrarily fix some parts of the curve in order to get integrable results. Note that here the unstated curves here do not require as much arbitrary correction.

Below are the tabular results that I have produced for various different setups. We begin with my first original trial, a specially weighted mean function that additionally includes a straight cut when the function grows larger than the strength (s.) parameter. This trial is considered a simplified version of the second trial which uses the same function but includes a weighted cut based on the value of the function at that point. I consider this second trial to be the best estimate for this system and

Figure 5-8: Noise Filtering Curves

(a) Maximal Curve

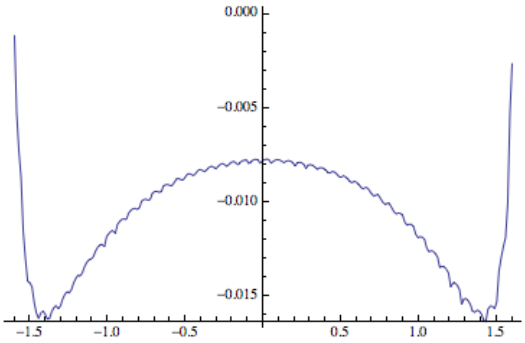

(b) Weighted Mean Curve (with additional smoothing)

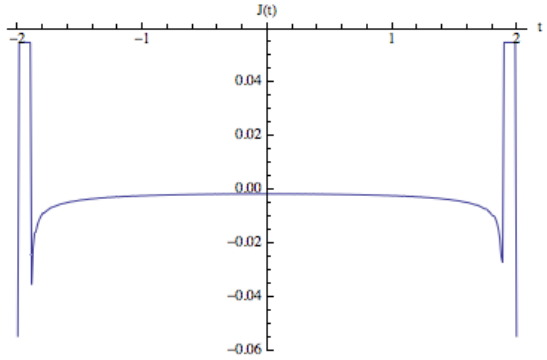

(c) Minimal Curve

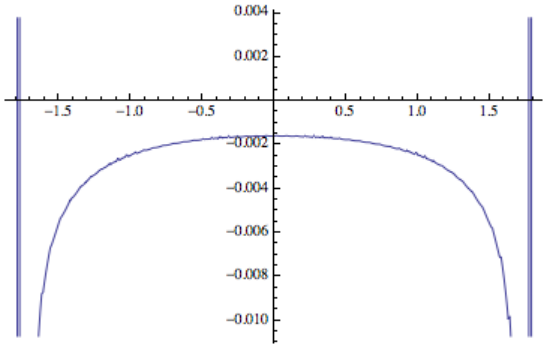

take its values to be the most accurate.

After these two trials, we have the trials from the maximal and minimal curve. As their names suggest, I have taken the two curves derived numerically above and applied straight cuts where necessary. Note that the exact mean trials are not included because the results are very similar to the maximal and original trial results. Also, the values of import are those with s. parameter between 0.055 - the limiting value from the tails - and 0.04 where the majority of the internal behavior is preserved.

5.4.2 Tabular Results

Original Trial 1		
S. Parameter	Backflow	% of Maximum
.055	-0.0331098	86.108
.05	-0.0332114	86.372
.04	-0.0333943	86.847
.03	-0.0315538	82.061

Original Trial 2		
S. Parameter	Backflow	% of Maximum
.055	-0.0330206	85.876
.054	-0.0331982	86.337
.05	-0.0332753	86.538
.04	-0.0334823	87.076
.03	-0.0334049	86.875
.02	-0.0329633	85.727
.01	-0.0308436	80.214
.005	-0.0270056	70.233

Minimal Curve Trial		
S. Parameter	Backflow	% of Maximum
.055	-0.0333437	86.716
.054	-0.0333558	86.747
.05	-0.0334304	86.941
.04	-0.0336306	87.462
.03	-0.0315528	82.058
.02	-0.0304692	79.240

Maximal Curve Trial		
S. Parameter	Backflow	% of Maximum
.055	-0.00767584	19.962
.05	-0.00769626	20.015
.04	-0.00771678	20.069

5.4.3 Discussion

Looking broadly at these results, we see that the maximum amount of backflow is produced with s. parameter near 0.04 and that for the weighted mean and minimal curves, the amount of backflow seems to be between 86.5% and 87.5%. Compared to the results from Yearsley et. al. (2012) and any other results in the literature to date, this result is at least a 16% improvement.

Unfortunately, we can not simply pick the best results and disregard the worst, no matter how consistent they seem. If we look at the maximal curve trial, we find backflow approximately 20% of the maximum which is uninspiring. With such a poor result it would be easy to write off this entire trial as a failure, but there is a reason to support the previous findings.

Since the original, unaltered current is highly oscillatory, perhaps due to inherent properties of the involved functions, there should be some effective function that approximates the current well. In our above trials, the maximal curve is the worst effective function that one could devise as it certainly minimizes the amount of backflow

produced for the system. So if one sets up an Airy wavefunction with our prescribed parameters in momentum space, these calculations seem to show that the *minimum* negative probability flux seen in the resulting current is around 20%.

While it is doubtful that these trials will lead to the absolute correct analytical solution, hopefully they will inspire future trials that lead us closer. Due to the difference in maximum and minimum amounts of backflow for this system, I must state that the actual effective backflow is most likely near 50%. Additionally, if this system is compared to the ideal case, we see that the time axis and consequently the current need to be scaled in order to arrive at the required $t = \pm 1$ asymptotes seen in the literature.

In future trials, we may add more parameters to the initial momentum-space wavefunction to make it more tuneable for higher backflow, though this will take up much more computational power and may make calculations unacceptably long. The time needed for some of the provided calculations was on the order of hours and any increase to this would make for slow progress. Another option would be to try the Airy Bi(-x) function as it has similar features to the given one. I have invested a few days time as of writing on these additional trials but numerical difficulties have so far been insurmountable. Once I am able to normalize the Bi(-x) trials, it will be possible to compare them with the Ai(-x) trials given here. Due to their similarities, I expect an almost identical treatment and thus may turn to newer trials that show more promise.

Chapter 6

Literature Review

In order to gain a full understanding of our stated topic, it is necessary to bring up a few more topics. This chapter will contain information relating to the background and application of our results.

6.1 Wigner Function and Negative Probability

A topic that so far has been often mentioned and taken for granted in interpretation is the conceptualization of negative probability. As mentioned in [19], negative probability was formally developed by constructing "a mathematical theory of extended probability...which is defined for random events and can take both positive and negative real values". Though it seems a rather foreign concept, the author suggests that situations such as antiparticles appearing where particles should in part of a calculation call for use of negative probability. As long as the final answer is appropriately positive, we may allow processes where at "intermediate steps of calculation negative numbers appear" [23]. This is to speed up and make calculations more intuitive - often it has been compared to subtracting numbers and ending up with an intermediately negative value even though the final answer will be positive due to future additions.

Fundamentally, it has been asserted that negative probability stems from "incompatibility of the observables (in an uncertainty relation); since they cannot be

measured simultaneously, there is no experimental procedure for estimating a joint probability distribution" [24]. It seems to be a limitation as a result of the uncertainty relations and one that can not easily be overcome. In fact, due to this origin, "the condition (on negative probabilities) is that they must be such that they could come from the Fourier analysis of an everywhere positive function" [23].

As detailed in [23], it is useful to introduce the Wigner function with the following properties:

1. Defined as: $W(x,p) = \int \psi(x - y/2)exp(-ipy)\psi(x + y/2)\, dy$

2. W(x,p) is real

3. Its integral with respect to p gives the probability that the particle is at x

4. Its integral with respect to x gives the probability that the momentum is p

5. The average value of a physical quantity M is given by

$$\langle M \rangle = \int w_M(x,p)F(x,p)\, dx\, dp$$

   where w_m is a weight function depending upon the character of the physical quantity

Note that we still have a viable physical theory if we implement the uncertainty principle. Now if we want to restrict to only positive probabilities, the weight functions must be hermitian operators, i.e.

$$w(x,p) = \int X(x - Y/2)exp(ipy)X^*(x + Y/2)\, dY$$

where X is any function.

For example, it has been found that a "necessary and sufficient condition for the Wigner density W corresponding to the Schrodinger state vector ψ to be a true probability density is that ψ be the exponential of a quadratic polynomial" [24].

Now that we know Wigner functions can in some sense be thought of as the probability density for quantum calculations, it is important to mention some more characteristics. As seen in [25], "the admissible quantum densities that correspond to pure states can be described by those functions of two variables that can be uniquely described in terms of a function of one variable. This imposes on the function W(p,q) an extremely strong condition," - the familiar uncertainty relation. Likewise, it has been found that "only the Liouville equation for the joint probability density W(p,q,t)" works and thus corresponding equations for "W(q,t) or for W(p,t) cannot exist" [25]. However W(p,q) is consistent with the one-dimensional cases W(p) and W(q) and we can additionally write

$$W(p,q) = \int \rho\,(q + y/2\,,\, q - y/2)\, exp(-ipy)\, dy$$

so that "the quasiprobability density can be regarded as the Fourier transform of the density with respect to the difference variable" [25]. Further on we learn that in order to perform accurate calculations we require "pure states" so that the Wigner function is appropriately used. Note that we can define the quantum mechanical current used in our calculations as

$$J(X,t) = \int F(X,p,t)\frac{p}{m}\, dp \tag{6.1}$$

as seen in [13].

6.2 Time of Arrival Problems

In Allcock's original 1969 paper [1], backflow was originally discussed as a side issue, specifically why our classical time of arrival distributions could not be used in the quantum case. Since time of arrival is the original forum for discussion of backflow, let us discuss it further especially since "the goal of a fully satisfactory theoretical description...remains elusive" [15].

So where does backflow fit in this discussion? It has been found in the rest of this thesis that the current can be negative for a free quantum state with only

positive momentum components which necessarily invalidates "J(0,t) as a probability distribution even in the free particle case" [15].

One test solution that made some progress on this issue was Kijowski's distribution given by

$$\Pi(t;\psi(0)) = \left| \frac{1}{\sqrt{mh}} \int_0^\infty \sqrt{p}\, exp(-ip^2 t/(2mh))\, \langle p|\psi(0)\rangle \; dp \right|^2 \tag{6.2}$$

which was important because of its relation to the flux

$$\int \Pi(t)\, t\, dt = \int J(t)\, t\, dt$$

though there were some subtle issues that made it an incomplete solution [13].

An important point to know regarding this discussion is that a perfect quantum absorber is not so perfect. In classical mechanics, we can have instantaneous absorption in the perfect absorber case but for a quantum system, "the absorption length cannot be strictly zero" [15] and the absorber must reflect part of the incoming wave in order to satisfy our conservation equations. As a result, our probability distribution must account for this. If we allow that "the expectation value of the current operator...(can be) negative for this reflective part" [18], then we can make sure that our current is appropriately and consistently defined to account for the mentioned phenomenon.

While I will not have time to detail the entirety of the subject, another possible solution to this time of arrival problem involves using complex potentials to approximate the problem. From [14], the key is to use

$$exp(-iH\epsilon)P\, exp(-iH\epsilon) \ldots P\, exp(-iH\epsilon) \approx exp(-iH\tau - V_0\theta(-x)\tau) \tag{6.3}$$

where the left side is the desired result involving projection operators and discrete time steps and the right side is our approximation involving a complex potential step function. For large enough time step ϵ and potential V_0, we find that this is a good approximation.

The interesting result for our discussion is that when we look at the large V_0 limit and normalize the distribution as

$$\Pi_N(\tau) = \frac{1}{m\langle p\rangle}\langle\psi_f(\tau)|\hat{p}\delta(\hat{x})\hat{p}|\psi_f(\tau)\rangle \tag{6.4}$$

we find that the result is obviously independent of V_0! Perhaps this is the way to go for a future solution to the time of arrival problem, but as of yet it remains unsolved.

6.3 Applications of Backflow

One experimental realization of the quantum backflow effect that has much promise is found in [20] and is based upon Bose-Einstein condensates. In this paper, the authors propose a set up that allows for observation of backflow by using BECs in harmonic traps - something that could be easily implemented. The basic idea is to populate the states with two unequal momenta such that the wavefunction is given by

$$\Psi(x,t) = \psi(x,t)(A_1 + A_2 exp(iqx + i\phi)) \tag{6.5}$$

with ϕ being an arbitrary phase. It then follows from $\frac{m}{\hbar}J_\Psi(x,t) = (\nabla\theta)\phi_\Psi + \frac{1}{2}q[\phi_\Psi + |\phi|^2(A_2^2 - A_1^2)]$ that

$$\phi_\Psi^{crit}(x,t) = \frac{q}{q + 2\nabla\theta(x,t)}|\phi(x,t)|^2(A_1^2 - A_2^2). \tag{6.6}$$

Not only does this result correspond to a purely quantum phenomenon (as seen in the full derivation), but it provides measurement of backflow via density measurements. So if we have a given system that may exhibit backflow, we would only need to look at it's density and compare it to the critical density to see whether it is applicable.

After discussion of an easy experimental setup, we can implement this system

with BECs with a wavefunction of the form

$$\psi(x,t) = \frac{1}{\sqrt{b(t)}}\psi_0(\frac{x - v_1 t}{b(t)})exp[ic_1(t)x^2 + ic_2 x + i\beta(t)] \tag{6.7}$$

where the function b(t) is the scaling parameter, β(t) is a global phase and c_1 and c_2 are related to b and its time derivative. As the authors state themselves, "eventually backflow can be probed by taking a snapshot of the interference pattern just after the Bragg pulse, measuring precisely its minimum and comparing it to the critical density".

Note that classical effects can lead to negative flux but these are due to repulsive interparticle interactions and may be omitted if appropriate wavefunction parameters are chosen. Additionally, the authors calculated that for a Li-7 experimental setup, backflow could be detected "with an imaging resolution of about 3 μ-m", which allows for practical observation.

Another reasonable application of backflow comes from [16] where the author presents a case for backflow arising in systems where an electron is placed in a magnetic field. By using basic equations and principles, the author makes this realization accessible to undergraduates. As he states himself: "For an electron in a magnetic field, it is possible to set up wavepackets composed entirely of states with negative values of the angular momentum quantum number which nevertheless have regions of space where the effective angular momentum is positivethese regions of backflow can, in principle, be sustained indefinitely". Since this setup could realistically be set up, this is a significant result. Note that the principle that is used is not position v. time uncertainty but azimuthal angle v. angular momentum uncertainty as we would expect for a spherically symmetric system like this.

Specifically, the author presents his quantum current as:

$$j(r,t) = \frac{\hbar}{2im}\left(\psi^*(r,t)\nabla\psi(r,t) - \psi(r,t)\nabla\psi^*(r,t)\right) - \frac{eA}{m}|\psi(r,t)|^2 = j_1 + j_2. \tag{6.8}$$

where j_1 is the quantum and j_2 is the classical contribution to the current. He

then derives the effective quantum number for angular momentum $m_{eff} = \frac{j_1}{\rho}$. The importance here is that the probability density is never negative ergo the effective angular momentum is always in the same direction as the quantum current. Because of the interplay between these quantities and the uncertainty relation that applies, backflow is produced. With very simple wavefunctions, for example

$$\psi_0(r) = c_0(r) + c_1(r)exp(-i\phi) + c_2(r)exp(-2i\phi)$$

the author is able to produce tangible backflow producing results. And while these simple cases may not seem important, they are notable because it is trivially easy to generalize them to the hydrogen atom case.

Chapter 7

Concluding Statements

From the first principles laid out in the time-of-arrival problem, we have developed here a numerical guide to backflow calculations. By analyzing the eigenvector and associated eigenvalue of the ideal system, we are able to gain an intuitive understanding of the system that can be used in adjusting models. With the help of MATLAB and Mathematica, I believe this framework can lead to an even better numerical approximation than the possible 87% solution found here.

Given more time, I would perform further analysis not only on my Airy trials but also on different functions. The Airy trials could benefit from more complicated dependence on the momentum inside the Airy function or perhaps some linear combination with the Airy Bi function. Additionally, noting the source of the Airy functions, it could be possible that the solution is a separate trigonometric integral, i.e. the solution to a different but related differential equation. I cannot think of an easy implementation, but searching through families of such functions would likely yield improved results.

Since the Airy functions may in fact be coincidentally good approximations to the backflow eigenvector, it is certainly possible that the correct solution is unrelated in origin. Looking for other oscillatory functions that fit this problem have been challenging for me, though again there may be a way to model this behavior that I am not aware of. The major gap that must be addressed is the one between numerical studies and theory, a gap that is widening. Even though our numerical results

are getting closer and closer to the ideal case, it will not be meaningful unless we can formulate a theory for the origin of the functions. After all, the reason we use these approximations instead of the ideal eigenvector is because we are looking for a physically realizable solution.

Though this thesis runs short on conclusion due to the open nature of the problem at hand, I think that I have provided enough information to an interested reader to go off and reproduce some important results. Since this problem is rarely studied, perhaps this thesis will serve as inspiration for a future discovery.

Chapter 8

Acknowledgements

Thanks to Professor Halliwell for his support and guidance especially with the circumstances I was dealing with this summer. Without his encouragement, I never would have known about this fundamental open question in quantum mechanics. I hope that we will someday figure out what it is that we're missing here to close this open chapter.

A final statement of thanks to Imperial College for a year of challenging courses and experiences, especially the world-class professors who so brilliantly instructed me. Though I am moving on to experimental physics, I hope that the knowledge gained this year will propel me to greatness.

Appendix A

Power Method Implementation

In this appendix, I will show the code I used to generate MATLAB plots and results as detailed by Penz. While the algorithm was presented to me, I have made subtle changes for accuracy and plotting purposes.

A.1 Heaviside Function

By far the simplest part of this program is the Heaviside function as shown below; it is self explanatory.

```
function [y] = Heaviside(x)
y = (x > 0);
y = y + (x == 0)/2;
end
```

A.2 Fourier Transform

Though the built in fast Fourier transform and inverse (called fft and ifft) are encoded into MATLAB, a slight tweak was necessary for our purposes. Below you will see that F is either the transform or inverse based on the input arguments. It is necessary to process the vectors like this for computational speed and the result is that we can flexibly input our required information and get exactly what we need back.

```
function [k,F] = FT(x,f,dir)
N = length(f);
x0 = max(x);
L = max(x)-min(x);
k0 = linspace(0,2*pi*(N-1)/L,N)';
if dir >= 0
F = L/(N*sqrt(2*pi))*fftshift(fft(f)).*exp(+1i*x0*k0);
else
F = L/sqrt(2*pi)*ifft(ifftshift(f.*exp(-1i*x0*k0)));
end
k = linspace(-pi*(N-1)/L,pi*(N-1)/L,N)';
end
```

A.3 Backflow Operator

The most important subroutine in this appendix is definitely this one, the backflow operator. Using explicitly the algorithm and equations from Penz's work, we encode this operator as follows:

```
function v = BackflowOp(k,u)
persistent U
persistent invU
if isempty(U) || length(U)~=length(k)
U = exp(-1i*k.^2);
invU = exp(1i*k.^2);
end
u = U.*Heaviside(k).*u;
[x,v] = FT(k,u,-1); % inverse FT
v = 1i*sign(x).*v;
[k2,v] = FT(x,v,1); % FT
v = Heaviside(k2).*invU.*v;
```

```
v = imag(v);
end
```

A.4 Power Method Program

This is the culmination of our effort, with the resulting program printing out not only the maximum eigenvalue but also the eigenvector in both coordinate and momentum space, though some of the functions have been obscured for ease of presentation. Note that we still input a value h that controls the range of the integration and thus the accuracy of the program. Compared to the matrix method, I have found this program to run between 10 and 100 times faster, a significant improvement for large values of h.

```
function [lambda,delta,y] = penzpower(h)
N0 = 500;
q0 = 10;
iter = 5000;

N = N0*h;
q = q0*sqrt(h);

k = linspace(-q,q,2*N)';
y = ones(2*N,1);
y = y.*Heaviside(k);
z = zeros(2*N,1);

for n=1:iter,
    v = y/norm(y);
    y = v-BackflowOp(k,v);
    z(N:2*N-1) = (y(N:2*N-1)+y(N+1:2*N))/2;
    y=z;
```

```
end

l = v'*y;
lambda = 1-l;

y = y(N:2*N);
v = v(N:2*N);
NF = sqrt(sum(v.^2)*sum((y-l*v).^2));
delta = sqrt(NF);

end
```

Bibliography

[1] G.R. Allcock, Ann.Phys. 53, 253 (1969).

[2] G.R. Allcock, Ann.Phys. 53, 286 (1969).

[3] G.R. Allcock Ann.Phys. 53, 311 (1969).

[4] A.J. Bracken and G.F. Melloy, J.Phys. A27, 2197 (1994).

[5] A.J. Bracken and G.F. Melloy, Found.Phys. 28, 505 (1998).

[6] S.P. Eveson, C.J. Fewster and R.Verch, Ann.Inst. H.Poincare 6, 1 (2005).

[7] M. Penz, G. Grubl, S. Kreidl and P.Wagner, J.Phys. A39, 423 (2006).

[8] J.D. Dollard, Commun. Math. Phys. 12, 193 (1969).

[9] J.M. Yearsley, J.J. Halliwell, R. Hartshorn and A. Whitby, quant-ph/1202.1783v4 (2012).

[10] G. Golub and C. Van Loan, *Matrix Computations*, (1989) 2nd edition (Baltimore, MD: John Hopkins University Press).

[11] M. Panju, Waterloo Math. Rev. 1, 9 (2011).

[12] O.V. Besov, M.M. Dzrbasjan, V.N. Faddeeva, V.N. Kublanovskaja and V.B. Lidskii, American Math. Soc. Trans. 2, 40 (1964).

[13] J.G. Muga, R. Sala and J.P. Palao, quant-ph/9801043v1 (1998).

[14] J.J. Halliwell and J.M. Yearsley, J.Phys. A: Math. Theor. 43, 445303 (2010).

[15] J.G. Muga, J.P. Palao and C.R. Leavens, Phys. Lett. A 253, 21 (1999).

[16] P. Strange, Eur. J.Phys. 33, 1147 (2012).

[17] M.S. Muthuvalu and J. Sulaiman, Int. J.App. Math. 3, 77 (2011).

[18] S. Boonchui and A. Hutem, J.Phys A: Math. Theor. 46, 105305 (2013).

[19] M. Burgin, quant-ph/1008.1287 (2010).

[20] M. Palmero, E. Torrontegui, J.G. Muga and M. Modugno, quant-ph/1302.3373v2

[21] M. Abramowitz and I. Stegun, *Handbook of Mathematical Functions with Formulas, Graphs, and Mathematical Tables*, (1970, p. 448).

[22] C.M. Bender and S.A. Orzag, *Advanced Mathematical Methods for Physicists and Engineers: Asymptotic Methods and Perturbation Theory* (1999).

[23] R.P. Feynman, *Negative Probability* in Quantum Implications: Essays in Honour of David Bohm (1987, p. 235).

[24] R.L. Hudson, Reports on Math. Phys.6, 249 (1974).

[25] V.I. Tatarkii, Sov. Phys. Usp. 26, 311 (1983).